Research Article **Open Access**

Marina Yu. Smirnova, Aleksei S. Bobin, Svetlana N. Pavlova, Arcady V. Ishchenko, Aleksandra V. Selivanova, Vasilii V. Kaichev, Svetlana V. Cherepanova, Tamara A. Krieger, Marina V. Arapova, Anne-Cecile Roger, Andrzej Adamski, Vladislav A. Sadykov*

Methane dry reforming over Ni catalysts supported on Ce–Zr oxides prepared by a route involving supercritical fluids

https://doi.org/10.1515/chem-2017-0046
received July 20, 2017; accepted November 29, 2017.

Abstract: $Ce_{0.5}Zr_{0.5}O_2$ mixed oxides were prepared in a flow reactor in supercritical isopropanol with acetylacetone as a complexing agent. Variation of the nature of the Zr salt and the temperature of synthesis affected the phase composition, morphology and specific surface area of oxides. X-ray diffraction and Raman spectroscopy studies revealed formation of metastable t" and t' phases. Oxides are comprised of agglomerates with sizes depending on the synthesis parameters. Loading NiO decreases the specific surface area without affecting X-ray particle sizes of supports. Such sintering was the most pronounced for a support with the highest specific surface area, which resulted in the lowest surface content of Ni as estimated by X-ray photoelectron spectroscopy and in the formation of flattened NiO particles partially embedded into the support. The catalytic activity and stability of these samples in the dry reforming of methane were determined by the surface concentration of Ni and the morphology of its particle controlled by the metal-support interaction, which also depends on the type of catalyst pretreatment. Samples based on ceria-zirconia oxides prepared under these conditions provide a higher specific catalytic activity as compared with the traditional Pechini route, which makes them promising for the practical application.

Keywords: Ce-Zr-O oxide, synthesis in supercritical isopropanol, Ni loading, characterization, catalytic properties in methane dry reforming

1 Introduction

Dry reforming of methane (DR) is now attracting significant attention because it converts cheap greenhouse gases into syngas with a H_2/CO ratio that is most suitable for synfuel production [1]. Mixed ceria-zirconia oxides promoted by inexpensive Ni are considered promising catalysts of methane dry reforming due to their high activity, thermal and coking stability provided by a strong Ni-support interaction, and high mobility and reactivity of the support oxygen [2-11]. Coking stability is explained by the bifunctional mechanism of this reaction, where surface oxygen species generated by CO_2 dissociation on the reduced sites of the ceria-zirconia support rapidly migrate to the metal-support interface and react with activated CH_x species on Ni, transforming them into syngas, thus preventing their polymerization into coke precursors [9,11].

Since the metal-support interaction and bulk/surface oxygen mobility and reactivity strongly depend on the phase composition and real/defect structure of mixed ceria-zirconia oxides [2,5-7,12,13], the preparation routes that determine these properties must be properly optimized. Thus, in the case of a microheterogeneous ceria-zirconia oxide system characterized by a coexistence of phases or nanodomains enriched with Ce or Zr, respectively, a fast deactivation of Ni-loaded catalysts due to coking was observed [14]. This problem can be dealt with by doping a ceria-zirconia mixed oxide with rare-earth cations (thus increasing oxygen mobility by generation of oxygen

***Corresponding author: Vladislav A. Sadykov:** Boreskov Institute of Catalysis, Novosibirsk, 630090, Russia; Novosibirsk State University, Novosibirsk, 630090, Russia, E-mail: sadykov@catalysis.ru
Marina Yu. Smirnova, Aleksei S. Bobin, Svetlana N. Pavlova, Arcady V. Ishchenko, Aleksandra V. Selivanova, Vasilii V. Kaichev, Svetlana V. Cherepanova, Tamara A. Krieger, Marina V. Arapova: Boreskov Institute of Catalysis, Novosibirsk, 630090, Russia
Marina Yu. Smirnova, Aleksei S. Bobin, Arcady V. Ishchenko, Vasilii V. Kaichev, Svetlana V. Cherepanova, Tamara A. Krieger: Novosibirsk State University, Novosibirsk, 630090, Russia
Anne-Cecile Roger: University of Strasbourg, Strasbourg, F-67087, France
Andrzej Adamski: Jagiellonian University, Krakow, Poland

vacancies) as well as supporting Ni alloys with Co or Pt group metals (to prevent coke nucleation) [8-11].

Recently, a modified Pechini route (using ethylene glycol solutions [13]) and synthesis in supercritical alcohols with the addition of acetylacetone as a complexing agent [14] were shown to provide the required uniformity of the spatial distribution of Ce and Zr cations between mixed oxide nanodomains, which resulted in a high activity and coking stability of catalysts with Ni supported on undoped ceria-zirconia. Their performance was shown to depend on both the Ce/Zr ratio in mixed oxides and their synthesis parameters. Since synthesis of mixed oxides under supercritical flow conditions is apparently attractive for their broad-scale production required for practical applications, a detailed study of the effect of synthesis parameters on the real structure of Ni-loaded ceria-zirconia catalysts as related to their catalytic performance is required. In this paper, this effect was considered for the case of $Ce_{0.5}Zr_{0.5}O_2$ oxide synthesis in supercritical isopropanol with variation of the nature of starting Zr compounds, the synthesis parameters and the pretreatment conditions, while Ni loading (5% wt/wt) was fixed.

2 Experimental

2.1 Catalyst Preparation

Samples of $Ce_{0.5}Zr_{0.5}O_2$ oxide were prepared by solvothermal synthesis (SCS) using supercritical isopropanol (T_c = 235.1°C, P_c = 4.76 MPa) in a flow reactor as described [14]. $ZrOCl_2 \cdot 8H_2O$ (Reakhim, chemically pure grade), $Zr(OBu)_4$ (Alfa Aesar, 80% solution in n-butanol) and $Ce(NO_3)_3 \cdot 6H_2O$ (Vecton, analytical grade) were used as starting compounds. Ceria and zirconia solutions were prepared by dissolution of reagents in isopropanol (Reakhim, extra pure grade). A two-fold molar excess of acetylacetone was added into the Zr solutions. In the case of the zirconium oxychloride solution, a five-fold molar excess of formic acid (Vecton, 98% purity) was added as well. These precursor solutions were mixed in the ratio required for obtaining the final product with a Ce:Zr molar ratio of 1. The precursor solution was introduced into the reactor system at a flow rate of 5 ml/min using an ISCO Syringe pump 100DM (Hamilton Instrument). Isopropanol, preheated to 300°C, was also introduced, at a flow rate of 9 ml/min. The synthesis was carried out in the temperature range of 400-480°C under a pressure of 120-130 bar. The product was cooled down in a heat exchanger located after the reactor outlet and collected as a suspension. A solid product was separated from the mother liquor by decantation. Solid residues were dried and calcined under air at 600°C for 2 h to obtain samples marked as 'B' and 'Ch' (Table 1).

NiO was loaded by wet impregnation using an aqueous solution of $Ni(NO_3)_2$ $6H_2O$ (Vecton, analytical grade) also containing cerium nitrate and zirconium oxychloride with the total concentration 10 times less than the Ni content, with the aim of providing a better Ni-support interaction as described [14]. After drying by microwave heating, samples were calcined under air in a muffle furnace at 600°C for 2 h. The nickel content in the reduced catalyst was 5 wt.%.

2.2 Catalysts Characterization

2.2.1 Specific surface area

The specific surface area was estimated with a SORBI N.4.1 apparatus by the four-point BET method from the amount of adsorbed Ar determined by the thermodesorption technique. Prior to measurements, samples were pretreated at 200°C in a vacuum for 1 h.

2.2.2 X-ray diffraction (XRD)

XRD patterns were recorded on a D8 Advance diffractometer (Bruker, Germany) in the 2θ angle range of 20-85° with a 0.05° step size using $Cu_{K\alpha}$ radiation. The intensity was registered by a position sensitive detector, LynxEye. Quantitative phase compositions were determined by lattice constants refinement using TOPAS software. The average particle sizes of ceria-zirconia and nickel oxide were estimated by the Selyakov-Scherrer equation from the integral broadening of the most intensive (002) and (200) lines.

2.2.3 High Resolution Transmission Electron Microscopy (TEM) and Energy Dispersive X-Ray Spectroscopy (EDX)

Transmission electron micrographs were obtained with a JEM-2010 instrument (JEOL Ltd., Japan) operated at an acceleration voltage of 200 kV. To prepare samples for TEM studies, they were suspended in ethanol and deposited on a carbon coated Cu grid. The nickel (NiO) particle size was estimated by measuring the size of at least 150 particles. TEM/EDX investigation was performed using a JEM-2200FS microscope (JEOL Ltd., Japan) equipped with a

Cs-corrector and an EDX spectrometer (JEOL Ltd., Japan). The minimum spot diameter for the step-by-step line EDX analysis was ~1 nm with a step of about 1-2 nm. The Ce/Zr ratio in synthesized oxides (Ce/Zr_v) was estimated by X-ray fluorescence analysis (XFA).

2.2.4 Raman scattering spectra (RSS)

Raman spectra were recorded using a LabRAM HR Evolution RS spectrometer (Horiba, Japan) in the back scattering geometry with the 488 nm argon ion laser line. The radiation intensity was ~ 1 mW on the sample surface with ~ 2 micron spot size.

2.2.5 X-ray photoelectron spectroscopy (XPS)

The study of the surface chemical composition of samples was carried out using the X-ray photoelectron spectroscopy technique on a SPECS Surface Nano Analysis GmbH (Germany) spectrometer equipped with a PHOIBOS-150 hemispherical electron energy analyzer, a FOCUS-500 X-ray monochromator and an XR-50M X-ray source with a double Al/Ag anode. The core-level spectra were obtained using monochromatic AlKα radiation (hν = 1486.74 eV) and a fixed analyzer pass energy of 20 eV under ultrahigh vacuum conditions. Relative element concentrations were determined from the integral intensities of the core-level spectra using the cross-sections according to Scofield [15]. For detailed analyses, the spectra were fitted into several peaks after background subtraction by the Shirley method. The fitting procedure was performed using CasaXPS software. Powdered catalysts were fixed on a sample holder by means of double sided adhesive tape.

2.2.6 H_2 TPR

Reactivity of Ni-loaded samples pretreated in O_2 at 400°C was studied using temperature- programmed reduction (TPR) by H_2 (10% H_2 in Ar, feed rate 2.5L h^{-1}, temperature ramp from 25 to 900°C at 10° min^{-1}). The experiments were carried out in kinetic installations equipped with GC Tcvet-500 [13,14].

2.2.7 Catalytic activity

The catalytic performance of Ni/Ce-Zr-O samples in methane dry reforming (MDR) was studied in a plug-flow quartz tube reactor under atmospheric pressure at 7.5 ms contact time in the feed 5% CO_2 + 5% CH_4 in He with the step-like uprising and subsequent decreasing temperature varying in the range of 600-800°C. Concentrations of reagents and products were monitored continuously with a Test-201 gas analyzer (Boner, Russia) equipped with optical, IR and electrochemical sensors. Samples were pretreated at 500°C for 0.5 h either in 10% O_2/He (oxidized samples) or in 10% H_2/He (reduced samples) flows.

2.2.8 Temperature-programmed oxidation by O_2 (TPO)

After the MDR experiments, samples were cooled in a He flow purified from the oxygen admixture. Temperature-programmed oxidation experiments were carried out in a 0.5% O_2 in He stream (100 ml/min) while applying a temperature ramp of 5°C/min from 100 to 800°C. The amount and reactivity of carbon-containing species accumulated in samples during the MDR reaction were estimated by continuous analysis of CO_x emission by a Test-201 analyzer.

Ethical approval: The conducted research is not related to either human or animals use.

3 Results and Discussion

3.1 Structural characteristics

3.1.1 XRD

Table 1 lists designations of samples as well as their structural and textural characteristics. Figure 1 displays diffraction patterns of Ce-Zr supports and Ni-loaded samples. For sample Ch, the metastable tetragonal t' phase with c/a < 1.01 is detected as the main phase (> 95%) (Table 1). A strong broadening of diffraction peaks observed in the patterns of B1 and B2 samples complicates their phase analysis. The full profile analysis (not shown in detail for the sake of brevity) reveals that such a broadening is not due to a small X-ray particle size but stems from a high level of microstrains in the structure of B1 and B2 supports. This fact suggests a coexistence of several solid solutions with a close chemical composition or even Ce/Zr gradient within oxide nanodomains. The refinement of the lattice parameters of B1 and B2 samples with regard to microstrains allows us to identify the metastable tetragonal t' phase (> 90%) and the cubic phase in their composition, respectively (Table 1).

Table 1: The synthesis conditions, phase compositions and textures of Ni/Ce-Zr-O samples.

Sample	Ce, Zr precursors	T_{scs}, °C	Ce/Zr[1]	Oxide structure[2]	D[3], nm	$S_{sp.}$[4], m^2/g	$S_{sp.}$[5], m^2/g
Ni/B1	$Ce(NO_3)_3$, $Zr(OBu)_4$	400	1.1	93T'+4C+3T	4	22	15
Ni/B2	$Ce(NO_3)_3$, $Zr(OBu)_4$	480	1.1	T''	5	57	20
Ni/Ch	$Ce(NO_3)_3$, $ZrOCl_2$	440	1.3	96T'+4C	8	21	19

1 – Ce/Zr ratio calculated using XFA data, 2 – phase composition (in %) determined by XRD and Raman spectroscopy, 3 – average crystallite size of the initial supports and CeZrO oxides in Ni/Ce-Zr catalysts, 4 – surface area of Ce-Zr oxide, 5 – surface area of Ni/Ce-Zr-O catalyst.

NiO loading does not affect the phase composition or dispersion (X-ray particle size) of ceria-zirconia oxides (Table 1). For NiO-loaded samples, along with CeZrO peaks, one can see three strongest reflections of the NiO phase (Figure 1). For all the samples, the average size of NiO crystallites estimated from broadening of the most intensive NiO line (200) at 43.25° lies in the range of 15 to 29 nm (Table 2).

3.1.2 Raman

Since the XRD method is sensitive mainly to the cation sublattice, Raman spectra were used to detect variation in the oxygen sublattice, thus distinguishing the t'' phase from the cubic phase. The t'' phase is characterized by the cation sublattice of the fluorite type and a tetragonal distortion of the oxygen sublattice [16-18]. In the Raman spectrum of sample B2, along with the band at 470 cm^{-1}, which is typical of the fluorite structure [17], the peaks at 300 and 620 cm^{-1} are observed. These peaks assigned to the t'' phase indicate some distortion of the oxygen sublattice [18]. For sample Ch, the presence of two extra bands at 192 and 595 cm^{-1} identifies the t′ phase [19], which agrees with XRD data. The Raman spectrum of sample B1 can be considered as a superposition of those corresponding to t′ and t phases with the band at 246 cm^{-1} indicating the presence of t phase.

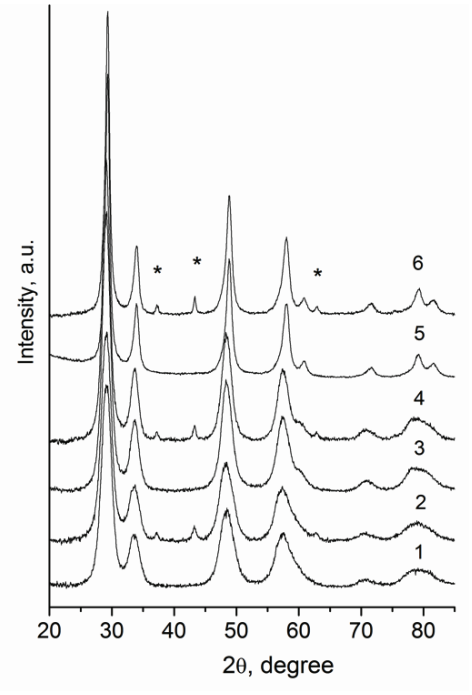

Figure 1: Powder XRD patterns of Ce-Zr supports (1, 3, 5) and Ni-modified samples (2, 4, 6): 1 – B1, 3 – B2, 5 – Ch, * – NiO reflections.

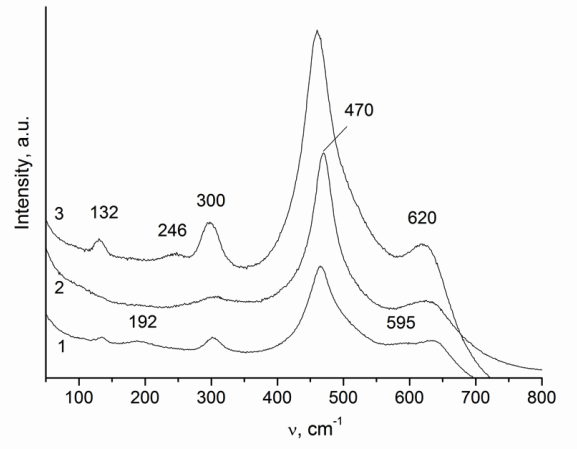

Figure 2: Raman spectra of the initial Ce-Zr supports: 1 – Ch, 2 – B2, 3 – B1.

3.2 Morphology and specific surface area

The morphologies of mixed ceria-zirconia oxides are shown in Figure 3. All samples are comprised of primary particles aggregated into nearly spherical agglomerates of varying sizes and degrees of aggregation. The agglomerates in sample B1 prepared at 400°C have the biggest size and a low degree of aggregation. The increase of synthesis temperature to 480°C reduces the size of agglomerates

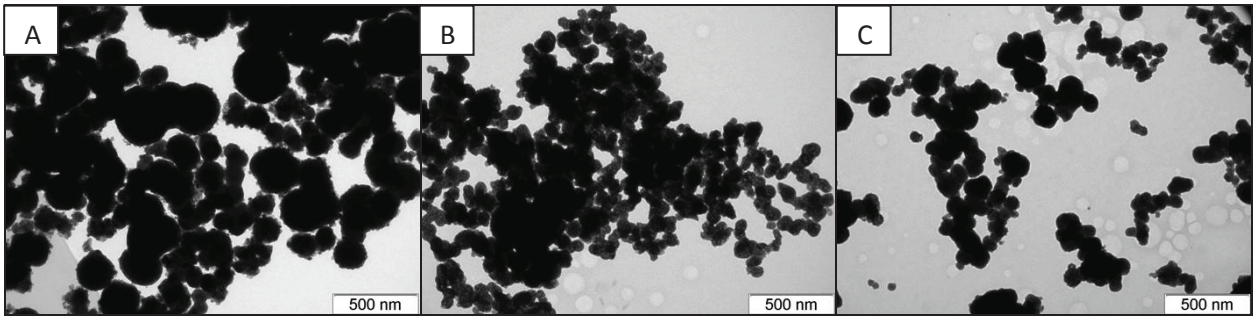

Figure 3: TEM images of the initial Ce-Zr supports: A - B1, B – B2, C – Ch.

Table 2: Average sizes of Ni-containing particles by TEM and XRD.

Sample	Average particle size of NiO (XRD), nm	Mean/median particle size of NiO (TEM), nm	Most probable D (TEM), nm	Particle size of Ni-NiO in the reduced samples, nm
Ni/B1	15	23/21	18-23	n.d.
Ni/B2	23	26/24	16-21, 34	24/22
Ni/Ch	29	28/26	24-28	22/21

and increases the degree of their agglomeration. Sample Ch, synthesized using zirconium oxychloride, possesses the morphology intermediate between those of samples B1 and B2.

Specific surface areas of the oxide supports and catalysts are presented in Table 1. Sample B2 has the highest specific surface area, which is consistent with smaller aggregate sizes.

For all samples studied, the specific surface area declined after NiO loading followed by calcination at 600°C. For sample B2, which possessed the highest initial specific surface area, such a decline is the most intense, but for all catalysts, specific surface areas are quite close, varying in the range of 15-20 m^2/g.

3.3 Morphology and size distribution of the nickel/nickel oxide particles by TEM

The catalyst samples examined by TEM were taken in three states: after preparation (in the oxidized state), after reduction and after testing in MDR. For all initial samples, the average sizes of NiO particles lay within a relatively small range of 23-28 nm (Table 2). It is worth noting that for sample N1/B2 these values are somewhat greater than those estimated by X-ray diffraction (Table 2). This difference may be caused by the presence of extended defects in NiO particles resulting in a decrease of the effective X-ray particle size [21].

High resolution TEM images of NiO particles (Figure 4) demonstrate that interaction with the oxide support depends on the sample. Thus, for samples Ni/B1 and Ni/Ch, NiO particles appear to have a rather small contact with the support, while in sample Ni/B2, their shape is flattened and they are in part embedded into the surface layers of CeZrO oxide, which suggests a stronger interaction with the support. The embedment of NiO particles into the ZrO_2 crystals due to calcination of the catalysts prepared by wet impregnation, with the formation of diffused interfacial region and not a sharp metal-support interface, was observed previously [22].

Investigation of samples Ni/Ch and Ni/B2 after the reducing treatment showed that the average size of Ni particles was close to that of NiO (Table 2). Furthermore, Ni particles in Ni/Ch were flattened, suggesting their stronger interaction with the support. The analysis of the interplanar distances in TEM images revealed the core-shell structure of Ni-containing particles consisting of the metal core and NiO shell. For sample Ni/B2, the surface of some Ni particles is covered by Ce-Zr-O layers (Figure 5B).

EDX scanning from the surface into the bulk of particles confirmed assumptions about the structure of Ni-containing particles in samples Ni/Ch and Ni/B2. Typical results such as those presented in Figure 6 demonstrate that the surface layer of Ni-containing particle in Ni/Ch is comprised mostly of Ni, while in Ni/B2 it is enriched with Ce and Zr.

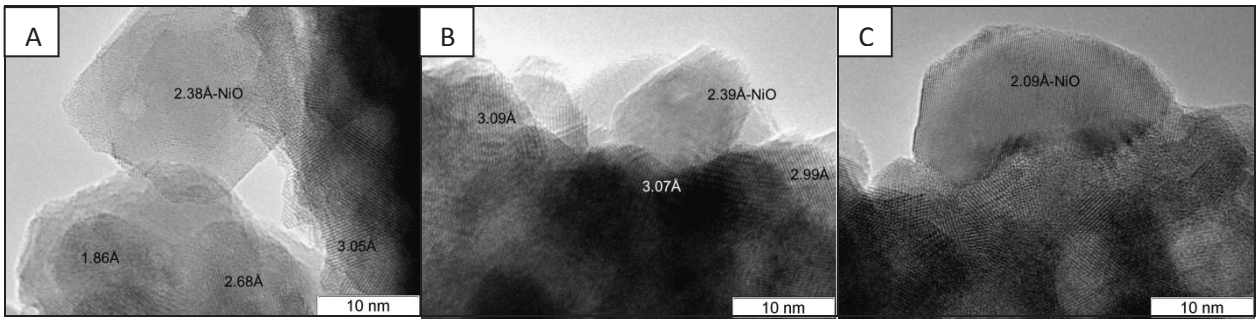

Figure 4: TEM images of calcined under air Ni/Ce-Zr catalysts: A - Ni/B1, B - Ni/Ch, C - Ni/B2.

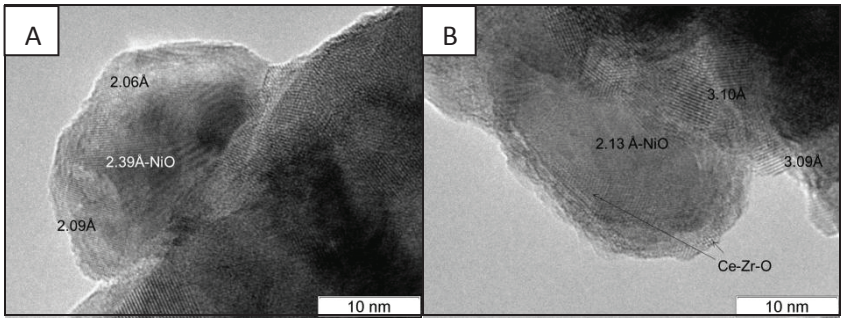

Figure 5: TEM images of Ni/Ce-Zr catalysts after reduction treatment: A - Ni/Ch, B - Ni/B2.

3.4 Surface composition

The results of XPS analysis of fresh and spent (AR) catalysts are summarized in Table 3. Note that the surface layer of B1 oxide is enriched by Zr in agreement with earlier published data for these parameters of the synthesis of mixed ceria-zirconia oxides in supercritical isopropanol [14]. However, increasing the synthesis temperature from 400 to 480°C (for sample B2) and the acidity of solutions by adding formic acid (for sample Ch) allows the surface concentration of Ce to be brought to the bulk level.

The Ni2p core-level spectra of fresh catalysts contain strong peaks characterized by the $Ni2p_{3/2}$ binding energy (BE) of 853.7-853.9 eV and corresponding to NiO (Figure 7). The component with a somewhat lower intensity at a higher BE 855.4-855.8 eV can be assigned to the surface Ni^{2+} cations incorporated into the surface positions of the oxide support [22,23]. The spectra of spent catalysts contain peaks at 852.3 eV (assigned to Ni in the metallic state), 853.7-853.9 eV (Ni^{2+} in the NiO structure) and 855.4-855.8 eV (Ni^{2+} in CeZrO layer, absent for Ni/B1) (Figure 7).

For the surface Ni concentration ([Ni]/[Ce+Zr]), the following order of samples was observed : Ni/B1 > Ni/Ch > Ni/B2 (Table 3). Since for all samples close average NiO sizes were revealed by TEM and specific surface areas

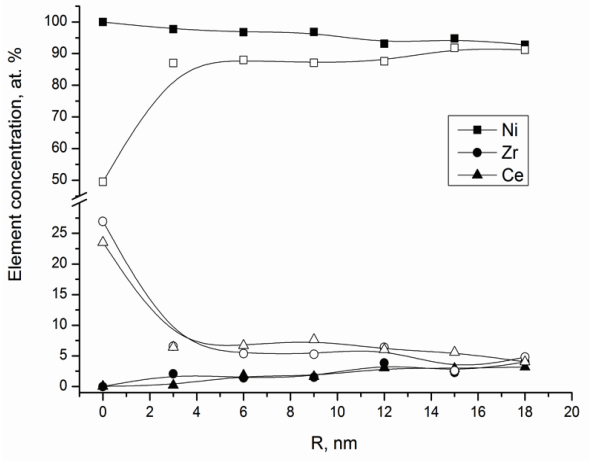

Figure 6: Ni, Ce, Zr distribution along the Ni-containing particle in samples Ni/Ch (solid symbols) and Ni/B2 (empty symbols). R - distance from the external surface to the center of the particle.

were close as well, the lowest surface concentration of Ni for sample Ni/B2 can be explained by strong sintering of the support after NiO loading leading to the pronounced decoration of NiO particles by the support fragments as well (vide supra Section 3.3). Studies of samples after their testing in the MDR reaction revealed a decline of the surface Ni content (Ni/Ce+Zr) for Ni/B1 and Ni/Ch catalysts

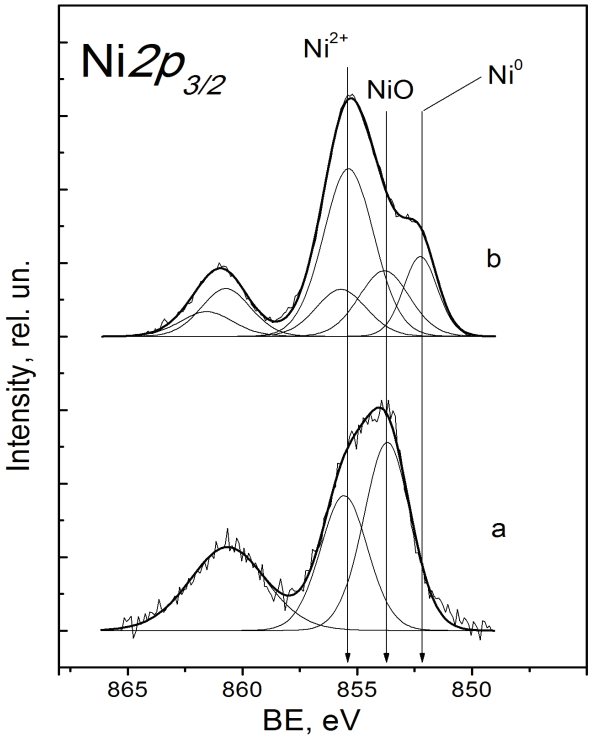

Figure 7: The Ni $2p_{3/2}$ core-level spectra for the Ni/B2 sample: a – fresh, b – spent.

(Table 3), which can be attributed to the presence of carbon nanotubes encapsulating Ni particles, as described below (Figure 10). For Ni/B2 sample Ni/B2, the surface Ni content after the reaction did not change, which is consistent with the absence of carbon nanotubes.

3.5 Reducibility

As follows from Figure 8a, the reduction of mixed ceria-zirconia oxides occurs in the temperature range of 300-900°C. For samples calcined at 600°C, the TPR profiles are characterized by one maximum shifted to a higher temperature for B1 and Ch with tetragonal structure. As the sintering temperature of supports is increased up to 800°C with respective decline of the specific surface area to ~ 10 m^2/g, the apparent reactivity decreases for support B2, while slightly increasing for other supports (Figure 8). Taking into account an increase in the average particle size of ceria-zirconia oxides after sintering at higher temperatures, this suggests a higher oxygen mobility in high-temperature CeZrO samples, which can be explained by a more uniform distribution of cations in oxide nanodomains [16,18]. For NiO-loaded samples, two overlapping TPR peaks are observed (Figure 8B). The first peak corresponds to reduction of loaded nickel oxide

Table 3: Atomic ratios of elements and relative Ni content in the near-surface layers of catalysts by XPS data.

Sample	$[Ce]/[Zr]_v$ by XRF	$[Ce]/[Zr]_s$	[Ni]/[Zr+Ce]	C(Ni^{2+} with BE of 855.4-855.8 eV), rel. %
Ni/B1	1.08	0.4	0.40	-
Ni/B1 AR		0.4	0.15	-
Ni/Ch	1.15	1.1	0.31	-
Ni/Ch AR		1.1	0.18	16
Ni/B2	1.11	1.0	0.11	-
Ni/B2 AR		0.9	0.11	50

with concomitant reduction of the surface layers of the supports, while the second peak is due to reduction of the bulk of ceria-zirconia oxide. Positions of the second peaks are shifted to lower temperatures as compared with those for pure supports, which is explained by H_2 activation/dissociation on Ni atoms and spillover of H atoms to the mixed oxide surface providing its fast reduction [24-26]. In all cases, H_2 consumption was higher than the calculated value for NiO reduction to Ni^0 (Table 4). For supported NiO catalysts, the position and shape of the first peak are determined by the reactivity of NiO, which is controlled by its dispersion, real/defect structure and interaction with the support [3,25-32]. Thus, for specially prepared bulk NiO samples, position of the reduction maximum varies from 280 [29] to 330-360 [3,28,30] or even 400-500ºC [26,31]. A strong interaction between NiO and the support results in a higher reduction temperature [3,26]. Highly dispersed NiO particles or isolated/clustered Ni cations on the surface of the support are reduced at temperatures < 300ºC [25,26]. For studied NiO/Ce-Zr-O samples, a complex shape of the first peak suggests coexistence of isolated Ni cations, their clusters and NiO particles on the surface of supports in agreement with UV-Vis spectra for similar catalysts [13]. Positions of the first TPR peak are quite close for samples studied here, while its intensity is the highest for sample Ni/Ch. The biggest separation of two TPR peaks is observed for sample Ni/B2, implying the lowest bulk oxygen mobility in support domains and/or rate of migration of surface oxygen species from the support to metal particles.

3.6 Catalytic properties

Catalyst testing was carried out by increasing the temperature from 600 to 800°C and subsequent decreasing

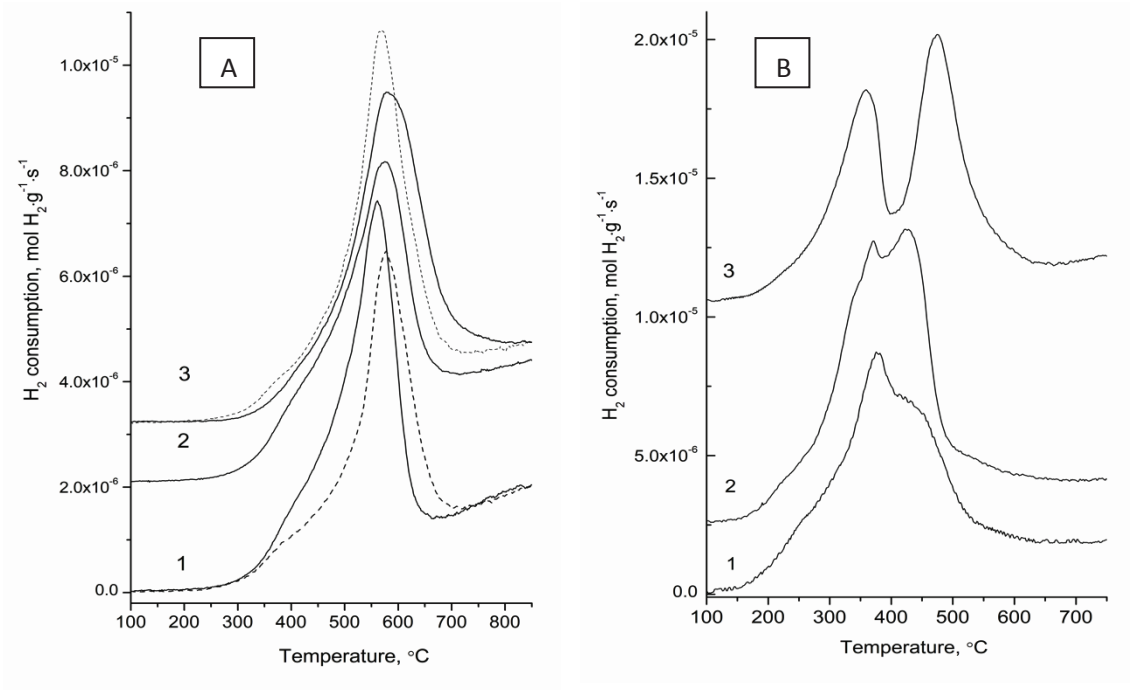

Figure 8: TPR profiles of the initial supports (A) calcined at 600°C (solid line) or 800°C (dashed line), and Ni/$Ce_xZr_{1-x}O_2$catalysts (B): 1 – B2 (Ni/B2), 2 – B1 (Ni/B1), 3 - Ch (Ni/Ch).

Table 4: TRP data of various Ni/Ce-Zr-O catalysts and initial supports.

Sample	H_2 consumption for the initial support, mmol H_2/g [1]	T max[2], °C	H_2 consumption for the catalyst, mmol H_2/g ct[4]	T max[5], °C	H_2/Ni
Ni/B1	1.35	573/566[3]	2.01	378, > 410 (shoulder)	2.37
Ni/B2	1.30	561/578[3]	1.93	359, 475	2.27
Ni/Ch	1.25	581/567[3]	2.19	371, 428	2.58

[1] – in the temperature region of 200-800°C, [2] – in TPR profiles of supports, [3] – for supports calcined at 800°C, [4] – in the temperature range of 100-700°C, [5] – in TPR profiles of catalysts

down to 600°C. For all oxidized samples, an abrupt burst of activity was observed at 650°C (Table 5). For catalysts pre-reduced by H_2, the catalytic activity was observed already at 600°C (Table 5). Conversions of reagents and the H_2/CO ratio increased with temperature for all samples (Figure 9). Upon subsequent temperature decrease from 800 to 600°C, conversions of reagents were reproduced for samples Ni/B1 and Ni/Ch, while for catalyst Ni/B2 a decline of activity was observed (Figure 9).

According to the initial value of CH_4 conversion at 650°C, the following order of sample activity was obtained: Ni/B1(74.6%) > Ni/Ch(67.9%) > Ni/B2(62.0%). This order of activity correlates with the surface nickel concentration derived from XPS data (Table 3). A similar trend was observed for stability of catalytic activity defined as the difference between the methane conversion at 650°C in the temperature cycle 600-800-600°C : Ni/Ch(4.4%) > Ni/B1(7.6%) >> Ni/B2(25.8%). Hence, carbon accumulated for the first two samples (Table 5) as nanotubes (Figure 10) appears to be "nontoxic". Note that decrease of the surface concentration of Ni estimated by XPS for samples Ni/B1 and Ni/Ch after reaction (Table 3) was not accompanied by a decline of activity in the temperature cycle (Table 5, Figure 9), thus implying that real/defect structure of Ni surface sites and their interface with support play a substantial role in catalytic performance of these systems.

Along with a lower activity and stability, catalyst Ni/B2 also demonstrates a reduced H_2/CO ratio (Table 5) due to the reverse water gas shift (RWGS) reaction [3]. Though it clearly operates for all samples, the difference between CH_4 and CO_2 conversion decreases with the increase in catalysts activity (Table 5).

As follows from Table 5, reduction pretreatment only slightly affected the catalytic activity of samples Ni/

Table 5: Catalytic data for Ni/Ce-Zr-O samples.

Sample	$X(CH_4)$ at T (°C), %			$X_r(CH_4)_{800}$-$X_{ox}(CH_4)_{800}$	$X(CO_2)_{800}$-$X(CH_4)_{800}$	H_2/CO at T (°C)			W(C)*, g_C/g_{Ct}
	600↑	800	600↓			600↑	800	600↓	
Ni/B1	-	91.9	50.2	2.0	1.3	-	0.91	0.85	0.12
Ni/B1 r	52.8	93.9	51.0		0.6	0.77	0.91	0.84	0.12
Ni/Ch	-	88.6	48.0	2.8	0.1	-	0.91	0.88	0.20
Ni/Ch r	58.0	91.4	52.3		0	0.80	0.93	0.88	0.12
Ni/B2	-	75.5	22.2	−4.5	4.0	-	0.86	0.71	-
Ni/B2 r	35.6	65.0	20.0		4.4	0.70	0.81	0.71	-

↑- during temperature increase; ↓ - during temperature decrease; * - estimated by TPO

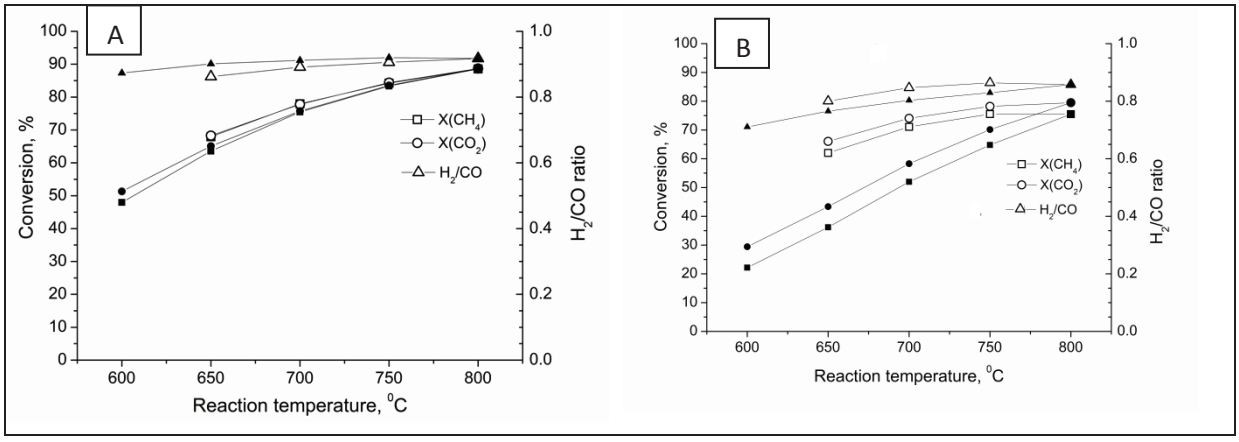

Figure 9: CH_4, CO_2 conversion and H_2/CO ratio for Ni/Ch (A) and Ni/B2 (B) in direct (empty symbols) and back (solid symbols) cycles.

B1 and Ni/Ch and even improved it, but it decreased the activity of catalyst Ni/B2. For catalyst Ni/B2, this effect can be assigned to a partial screening of the Ni surface by reduced fragments of the support, which agrees with TEM EDX data.

Estimation of specific first-order rate constants for the samples under study (Table 6) using the integral equation for the plug-flow reactor [14] revealed that Ni-loaded catalysts based on ceria-zirconia supports prepared in supercritical isopropanol are substantially more active than catalysts based on ceria-zirconia prepared by the modified Pechini route using ethylene glycol solutions. This correlates both with the higher oxygen mobility in SC catalysts estimated by H_2 TPR (several times higher peak rates for both peaks) and a higher surface concentration of Ni after the reaction (0.11-0.18 vs. 0.066 in [13]). Moreover, Ni-loaded catalysts on ceria-zirconia supports prepared using water solutions were even less active (up to 2 orders of magnitude) due to deactivation by carbon deposition explained by a pronounced microheterogeneity of supports [11]. This again demonstrates a high sensitivity of activity of Ni-loaded ceria-zirconia catalysts in MDR to their real structure and texture as controlled by the method of synthesis. In a similar way, a Ni-$Ce_{1-x}Zr_xO_2$ catalyst prepared by surfactant assisted co-precipitation was found to be not active at all in MDR due to encapsulation of Ni particles by the ceria-zirconia support, while catalysts prepared without a surfactant were reasonably active [4]. In our case, a partial encapsulation was found to play a role as well, although the effect was apparently much less pronounced.

Hence, the most important and novel result of this research is that synthesis of mixed ceria- zirconia oxides in supercritical isopropanol with the addition of acetyl acetone as a complexing agent allows the production of single-phase samples with a high oxygen mobility and reactivity and strong interaction with supported Ni. This method of synthesis provides uniquely high activity and coking stability of these catalysts in MDR, which have not been achieved to date using any other (including even Pechini) methods without doping catalysts with precious metals. This opens the attractive possibility of using this

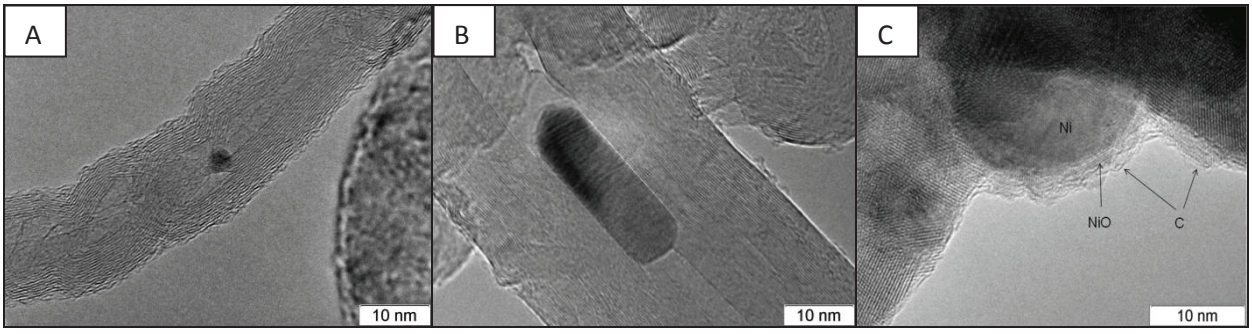

Figure 10: TEM images of Ni/Ce-Zr catalysts after MDR: A-Ni/B1, B-Ni/Ch, C-Ni/B2.

Table 6: Comparison of specific catalytic activity of 5%Ni/$Ce_{0.5}Zr_{0.5}O_2$ samples at 600°C.

Sample	X(CH_4),%	K, $s^{-1}m^{-2}$
Ni/Ch	48	4.1
Ni/B2	23	1.6
Ni/$Ce_{0.5}Zr_{0.5}O_2$ Pechini [13]	12	0.35

route for preparation of such catalysts for broad practical applications.

3.7 Post-reaction characterization

3.7.1 Textural features

For samples Ni/Ch and Ni/B1 post-reaction, many carbon nanotubes as well as small Ni nanoparticles with diameters less than 10 nm were observed (Figure 10).

Effects of the formation of Ni nanoparticles under MDR reaction conditions were observed by Martinez et al. [33] and assigned to strain-induced separation from larger particles. In their opinion, the contribution of such nanoparticles to the activity is minor due to trapping by carbon filaments [33]. However, for some supports, the appearance of Ni nanoparticles due to reduction of Ni cations incorporated into the surface layers of oxides and their clustering via surface migration could not be excluded [13].

For sample Ni/B2, the total amount of carbon was much lower, and only amorphous carbon deposition was observed. In some places, carbon deposition was located on Ni particles and adjacent support areas (Figure 10).

The relationship between the amount of deposited carbon and the metal particle size has been discussed extensively [32,34,35]. For sufficiently small (< 6-10 nm) nickel particles, carbon filaments are not formed [33,36,37]. For samples studied in this work, the appearance or absence of carbon nanotubes is not controlled by Ni particle size. Two possible reasons for generation of carbon fibers on samples Ni/B1 and Ni/Ch can be considered: a lower reactivity of surface oxygen species or an alternative morphology of Ni particles (namely, specific crystallographic plane orientation). Roh et al. pointed out that the enhanced activity and improved stability of Ni/Ce-Zr-O catalysts with a high Ce concentration could be explained by a higher oxygen storage capacity of cubic $Ce_{0.8}Zr_{0.2}O_2$ in comparison with the other Ce-Zr-O phases [6]. Moreover, Marki et al. emphasized that an improvement in the rate of oxygen transfer from the support towards the Ni-support interface is more important than the increase of oxygen storage capacity [10].

In comparing the performance of Ni/Al_2O_3 catalysts in MDR, Juanjuan et al. proposed that not only the particle size but also the particle morphology (structure) determined carbon deposition [32]. The effect of the morphology of Ni particles on their coking in MDR was also discussed by Kroll et al. [38]. The authors proposed that the appearance of faceted and flat particles in Ni/SiO_2 catalysts could favor the carbon excretion along certain planes without particle encapsulation, in contrast with samples in which particles do not have any specific plane orientation. The combination of microfacets on the surface of near spherical particles is expected to favor undirected carbon growth around the particle and, hence, isolation of the metal surface from reagents.

Along with Kroll et al., many authors considered carbon filaments as "nontoxic carbon", since even at a large amount of this carbon accumulation the catalyst maintains its activity for an extended period [4,39-40]. In agreement with these results, the activity of catalysts Ni/B1 and Ni/Ch decreased only slightly despite a considerable carbon accumulation. Nevertheless, XPS data revealed some decrease in the Ni surface concentration, which could provide evidence for a partial shielding of the Ni surface by carbon. This shielding may be due to the presence of some

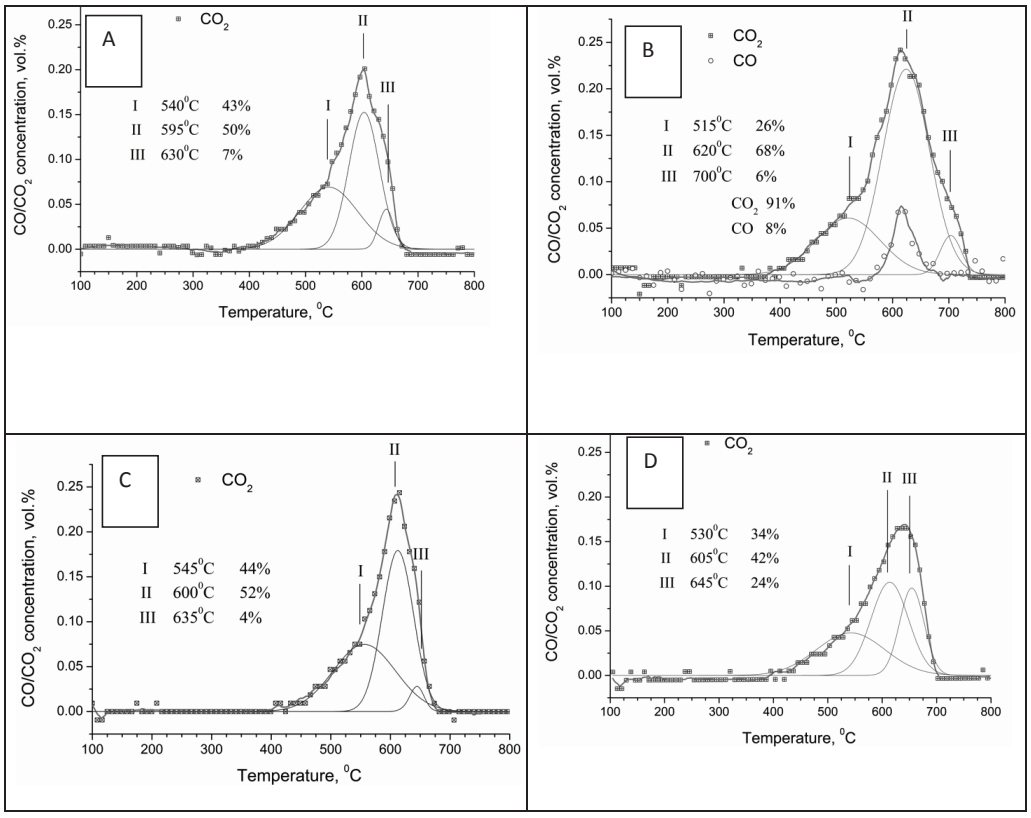

Figure 11: CO_2 production during TPO in 0.5% O_2 in He after MDR for samples Ni/B1 (A, C) and Ni/Ch (B, D) as prepared (A, B) and reduced (C, D).

graphitic carbon or filaments overlapping encapsulated Ni particles (Figure 10A). In any case, for the practical application of these catalysts, the formation of carbon filaments is to be suppressed, since eventually it will result in the plugging of the reactor. Following approaches developed earlier [11], carbon filament suppression can be achieved by doping the surface of ceria-zirconia oxides with Pr^{3+}/Pr^{4+} cations and adding some amount of Ru to dilute ensembles of Ni atoms on the surface of metal particles.

3.7.2 Temperature programmed oxidation

Figure 11 presents the TPO curves for catalysts Ni/B1 and Ni/Ch after the entire catalytic cycle including MDR reaction at both increasing and decreasing temperatures. For Ni/B2, carbon was not detected in these experiments due to its low amount. These results are in good agreement with the TEM data (Figure 10C), which reveal minimal carbon deposits on Ni/B2 after the reaction and the confinement these deposits only to some specific sites.

Fitting of experimental TPO curves demonstrated that both samples contain at least three types of carbonaceous species with different reactivity. According to published data [4], the amorphous carbon is oxidized at 300°C; the peak around 500°C can be assigned to the burn-off of graphitic carbon, and CO_2 evolution at ~ 600°C corresponds to the oxidation of whisker carbon. Along with CO_2 production, CO evolution was observed for sample Ni/Ch during the TPO run.

The estimation of the amount of carbon dioxide formed during the burn-off of each carbonaceous form revealed that for both samples the relative content of fibrous carbon is at least 50%. The samples also contain graphitic carbon as well as a small amount of carbon with a combustion temperature exceeding 620°C. It is possible that the high temperature peak originates from the decomposition of the carbonates [4]. It should be stressed that despite a large amount of accumulated coke, its removal by oxidation has not resulted in deterioration of activity and/or selectivity for samples Ni/B1 and Ni/Ch in repeated catalytic cycles.

Since the reducing pretreatment only slightly increases the activity of catalyst Ni/Ch and does not affect the performance of sample Ni/B1 (vide supra), TPO experiments were performed for these pre-reduced

catalysts after carrying out the catalytic cycles as well. For catalyst Ni/B1, the pre-reduction did not affect the shape of the TPO curve, while for catalyst Ni/Ch it decreased the total amount of coke, suppressed CO evolution and increased the fraction of the high-temperature component. Similar effects of the reducing pretreatment on the coke amount (its decrease for pre-reduced sample) were observed for catalyst Ni/Al_2O_3 and can be explained by the decreasing size of Ni particles and the variation of their morphology [32]. In our case, TEM has not revealed any noticeable variation of the average size of Ni particles after *ex-situ* reduction; hence, the decrease in the coke amount could be caused by variation of Ni particle morphology or their partial decoration by fragments of the support, thus decreasing the size of Ni atoms ensembles on the surface. A smaller size of Ni ensembles prevents carbon deposition because the size necessary for carbon nucleation is larger than that required for CH_4 reforming [41]. In any case, the most effective approach to decreasing Ni particle size is the use of perovskite-like or spinel complex oxide precursors, which are decomposed under the reaction conditions, producing Ni nanoparticles not subjected to coking [42]. Note that the addition of Ce and Zr salts to the impregnation solution has not helped to modify the surface properties of Ni particles required to prevent coke generation.

4 Conclusions

The synthesis of $Ce_{0.5}Zr_{0.5}O_2$ samples in a flowing supercritical isopropanol solution using different zirconium salts (butoxide, oxychloride) with the addition of acetylacetone as a complexing agent allowed us to obtain nanocrystalline mixed oxides with the tetragonal t' or pseudo-cubic t" structure and different textural characteristics. Increasing of the synthesis temperature increased the specific surface area of the powder prepared using zirconium butoxide. However, Ni loading on the support with the highest surface area resulted in some encapsulation of Ni particles. This process, along with the pronounced decoration of the surface Ni sites by the support species observed under the reducing conditions, decreases catalytic activity in MDR but presents several advantages such as negligible coking. A weaker Ni-support interaction was revealed for the catalysts based on supports prepared at lower temperatures, and resulted in the generation of fibrous carbon that did not deteriorate the catalytic performance but did threaten reactor plugging. TEM data implied that the nature as well as the amount of the carbon deposits in the spent catalysts were controlled by the structure of Ni particles rather than their average size.

All studied catalysts exhibited higher specific catalytic activities in MDR as compared to catalysts with similar chemical composition but prepared by the modified Pechini route. This is the most unique, novel and important result described in our paper. Thus, this research has demonstrated that synthesis in supercritical isopropanol is a promising route for preparing efficient MDR catalysts that are attractive for practical applications, though improvement of their resistance to coking via doping using known approaches could be useful as well.

Acknowledgements: Support by NICE project of ERA Net Rus Plus Call and Russian Ministry of Education and Science under related contract №14.616.21.0036 (unique identifier of the contract RFMEFI61615X0036) is gratefully acknowledged.

Conflict of interest: Authors state no conflict of interest.

References

[1] Verykios X. E., Catalytic dry reforming of natural gas for the production of chemicals and hydrogen, Int. J. Hydrogen Energy, 2003, 28, 1045–1063.
[2] Kambolis A., Matralis H., Trovarelli A., and Papadopoulou C., Ni/CeO_2-ZrO_2 catalysts for the dry reforming of methane, Appl. Catal. A-Gen., 2010, 377, 16–26.
[3] Montoya J. A., Romero-Pascual E., Gimon C., Del Angel P., and Monzón A., Methane reforming with CO_2 over Ni/ZrO_2–CeO_2 catalysts prepared by sol–gel, Catal. Today, 2000, 63, 71–85.
[4] Wolfbeisser A., Sophiphun O., Bernardi J., Wittayakun J., Föttinger K., and Rupprechter G., Methane dry reforming over ceria-zirconia supported Ni catalysts, Catal. Today, 2016, 277, 234–245.
[5] Chen J., Wu Q., Zhang J., and Zhang J., Effect of preparation methods on structure and performance of $Ni/Ce_{0.75}Zr_{0.25}O_2$ catalysts for CH_4-CO_2 reforming, Fuel, 2008, 87, 2901-2907.
[6] Roh H.-S., Potdar H. S., Jun K.-W., Kim J.-W., and Oh Y.-S., Carbon dioxide reforming of methane over Ni incorporated into Ce–ZrO_2 catalysts, Appl. Catal. A-Gen., 2004, 276, 231–239.
[7] Sukonket T., Khan A., Saha B., Ibrahim H., Tantayanon S., Kumar P., et al., Influence of the catalyst preparation method, surfactant amount, and steam on CO_2 reforming of CH_4 over $5Ni/Ce_{0.6}Zr_{0.4}O_2$ catalysts, Energy Fuels, 2011, 25, 864–877.
[8] Horvath A., Stefler G., Geszti O., Kienneman A., Pietraszek A., and Guczi L., Methane dry reforming with CO_2 on CeZr-oxide supported Ni, NiRh and NiCo catalysts prepared by sol-gel technique: relationship between activity and coke formation, Catal. Today, 2011, 169, 102–111.
[9] Khan A., Sukonket T., Saha B., and Idem R., Catalytic activity of various 5 wt.% $Ni/Ce_{0.5}Zr_{0.33}M_{0.17}O_2$- catalysts for the CO_2

reforming of CH_4 in the presence and absence of steam, Energy Fuels, 2012, 26, 365–379.

[10] Makri M. M., Vasiliades M. A., Petallidou K. C., and Efstathiou A. M., Effect of support composition on the origin and reactivity of carbon formed during dry reforming of methane over 5 wt% $Ni/Ce_{1-x}M_xO_2$-δ (M = Zr^{4+}, Pr^{3+}) catalysts, Part 1, Catal. Today, 2016, 259, 150–164.

[11] Bobin A. S., Sadykov V. A., Rogov V. A., Mezentseva N. V., Alikina G. M., Sadovskaya, et al., Mechanism of CH_4 dry reforming on nanocrystalline doped ceria-zirconia with supported Pt, Ru, Ni, and Ni–Ru, Topics in Catal., 2013, 56, 958–968.

[12] Mamontov E., Brezny R., Koranne M., and Egami T., Nanoscale heterogeneities and oxygen storage capacity of $Ce_{0.5}Zr_{0.5}O_2$, J. Phys. Chem. B, 2003, 107, 13007–13014.

[13] Sadykov V. A., Simonov M. N., Mezentseva N. V., Pavlova S. N., Fedorova Y. E., Bobin A. S., et al., Ni-loaded nanocrystalline ceria-zirconia solid solutions prepared via modified Pechini route as stable to coking catalysts of CH_4 dry reforming, Open Chem., 2016, 14, 363–376.

[14] Smirnova M. Yu., Pavlova S. N., Krieger T. A., Bespalko Yu. N., Anikeev V. I., Chesalov Yu. A., et al., Synthesis of $Ce_{1-x}Zr_xO_2$ oxides in supercritical alcohols and based on them catalysts for carbon dioxide reforming of methane, Supercritical Fluids: Theory And Practice, 2017, 12, №1, 15–28.

[15] Scofield J. H. J., Hartree-Slater subshell photoionization cross-sections at 1254 and 1487 eV, Electron Spectrosc. Relat. Phenom., 1976, 8, 129–137.

[16] Vlaic G., Di Monte R., Fornasiero P., Fonda E., Kašpar J., and Graziani M., Redox property–local structure relationships in the Rh-loaded CeO_2–ZrO_2 mixed oxides, J. Catal., 1999, 182, 378–389.

[17] Fornasiero P., Balducci G., Di Monte R., Kašpar J., Sergo V., Gubitosa G., et al., Modification of the redox behaviour of CeO_2 induced by structural doping with ZrO_2, J. Catal., 1996, 164, 173–183.

[18] Fornasiero P., Fonda E., Di Monte R., Vlaic G., Kašpar J., and Graziani M., Relationships between structural/textural properties and redox behavior in $Ce_{0.6}Zr_{0.4}O_2$ mixed oxides, J. Catal. 1999, 187, 177–185.

[19] Yashima M., Arashi H., Kakihana M., and Yoshimura M., Raman scattering study of cubic-tetragonal phase transition in $Zr_{1-x}Ce_xO_2$ solid solution, J. Am. Ceram. Soc., 1994, 77, 1067–1071.

[20] Kim D.-J., Jung H.-J., and Yang I.-S., Raman spectroscopy of tetragonal zirconia solid solutions, J. Am. Ceram. Soc., 1994, 76, 2106–2108.

[21] Ungár T. and Gubicza J., Nanocrystalline materials studied by power diffraction line profile analysis, Z. Kristallogr., 2007, 222, 114–128.

[22] Zou J.-J., Liu C.-J., and Zhang Y.-P., Control of the metal-support interface of NiO-loaded photocatalysts via cold plasma treatment, Langmuir, 2006, 22, 2334–2339.

[23] Lorenz P., Finster J., Wendt G., Salyn J. V., Zumadilov E. K., and Nefedov V. I., ESCA investigations of some NiO/SiO_2 and $NiO-Al_2O_3/SiO_2$ catalysts, J. Electron Spectrosc., 1979, 16, 267–276.

[24] Holgado J. P. and Munuera G., XPS/TPR study of the reducibility of M/CeO_2 catalysts (M=Pt, Rh): Does junction effect theory apply? Stud. Surf. Sci. Catal., 1995, 96, 109–122.

[25] Mahammadunnisa Sk., Manoj Kumar Reddy P., Lingaiah N., and Subrahmanyam Ch., $NiO/Ce_{1-x}Ni_xO_{2-\delta}$ as an alternative to noble metal catalysts for CO oxidation, Catal. Sci. Technol., 2013, 3, 730–736.

[26] Rao P. V. R., Kumar V. P., Rao G. S., and Chary K. V. R., Vapor phase selective hydrogenation of acetone to methyl isobutyl ketone (MIBK) over Ni/CeO_2 catalysts, Catal. Sci. Technol., 2012, 2, 1665–1673.

[27] Nichele V., Signoretto M., Menegazzo F., Gallo A., Dal Santo V., Cruciani G., et al., Glycerol steam reforming for hydrogen production: Design of Ni supported catalysts, Appl. Catal. B-Environ., 2012, 111–112, 225–232.

[28] Pérez-Hernández R., Gutiérrez-Martínez A., Palacios J., Vega-Hernández M., and Rodríguez-Lugo V., Hydrogen production by oxidative steam reforming of methanol over Ni/CeO_2-ZrO_2 catalysts, Int. J. Hydrogen Energy, 2011, 36, 6601–6608.

[29] Richardson J. and Twigg M., Reduction of impregnated NiO/α-Al_2O_3 Association of Al^{3+} ions with NiO, Appl. Catal. A-Gen., 1998, 167, 57–64.

[30] Sánchez-Sánchez M. C., Navarro R. M., and Fierro J. L. G, Ethanol steam reforming over $Ni/La–Al_2O_3$ catalysts: Influence of lanthanum loading, Catal. Today, 2007, 129, 336–345.

[31] Matte L. P., Kilian A. S., Luza L., Alves M. C. M., Morais J., Baptista D. L., et al., Influence of the CeO_2 support on the reduction properties of Cu/CeO_2 and Ni/CeO_2 nanoparticles, *J. Phys. Chem. C,* **2015**, *19* (47), 26459–26470.

[32] Juan-Juan J., Román-Martínez M.C., and Illán-Gómez M.J., Nickel catalyst activation in the carbon dioxide reforming of methane. Effect of pretreatments, Appl. Catal. A-Gen., 2009, 355, 27–32.

[33] Martínez R., Romero E., Guimon C., and Bilbao R., CO_2 reforming of methane over coprecipitated Ni–Al catalysts modified with lanthanum, Appl. Catal. A-Gen., 2004, 274, 139–149.

[34] Tang S., Ji L., Lin J., Zeng H. C., Tan K. L., and Li K., CO_2 reforming of methane to synthesis gas over sol–gel-made $Ni/γ-Al_2O_3$ catalysts from organometallic precursors, J. Catal., 2000, 194, №2, 424–430.

[35] Zhang J., Wang H., and Dalai A. K., Effects of metal content on activity and stability of Ni-Co bimetallic catalysts for CO_2 reforming of CH_4, Appl. Catal. A-Gen., 2008, 339, 121–129.

[36] Duprez D., DeMicheli M. C., Marecot P., Barbier J., Ferretti O. A., and Ponzi E. N., Deactivation of steam-reforming model catalysts by coke formation i. kinetics of the formation of filamentous carbon in the hydrogenolysis of cyclopentane on Ni/Al_2O_3 catalysts, J. Catal., 1990, 124, 324–335.

[37] Kim J.-H., Suh D. J., Park T.-J., and Kim K.-L., Effect of metal particle size on coking during CO_2 reforming of CH_4 over Ni–alumina aerogel catalysts, Appl. Catal. A-Gen, 2000, 197, 191–200.

[38] Kroll V. C. H., Swaan H. M., and Mirodatos C., Methane reforming reaction with carbon dioxide over Ni/SiO_2 catalyst. I. Deactivation studies, J. Catal., 1996, 161, 409–422.

[39] Zhang T. and Amiridis M. D., Hydrogen production via the direct cracking of methane over silica-supported nickel catalysts, Appl. Catal. A-Gen., 1998, 167, №2, 161–172.

[40] [40] San-José -Alonso D., Juan-Juan J., Illán-Gómez M.J., and Román-Martínez M.C., Ni, Co and bimetallic Ni–Co catalysts for the dry reforming of methane, Appl. Catal. A-Gen., 2009, 371, 54–59.

[41] Hu Y. H. and Ruckenstein E., Catalytic conversion of methane to synthesis gas by partial oxidation and CO_2 reforming, Adv. Catal., 2004, 48, 297–345.
[42] Sadykov V., Mezentseva N., Simonov M., Smal E., Arapova M., Pavlova S., Fedorova Y., Chub O., Bobrova L., Kuzmin V., Ishchenko A., Krieger T., Roger A.-C., Parkhomenko K., Mirodatos C., Smorygo O., Ross J., Structured nanocomposite catalysts of biofuels transformation into syngas and hydrogen: Design and performance, Int. J. Hydrogen Energy, 2015, 40, 7511–7522.